Pergamon

Int. J. Heat Mass Transfer. Vol. 40, No. 6, pp. 1313–1323, 1997

0017–9310/97 $17.00+0.00

PII: S0017-9310(96)00203-7

The Prandtl number effect on the optimum heating frequency of an enclosure filled with fluid or with a saturated porous medium

B. V. ANTOHE
MicroFab Technologies Inc., Plano, TX 75074, U.S.A.

and

J. L. LAGE†
Mechanical Engineering Department, Southern Methodist University, Dallas, TX 75275-0337, U.S.A.

(*Received* 5 *April* 1996 *and in final form* 29 *May* 1996)

Abstract—This is a fundamental study of the Prandtl number effect on the natural convection flow within an enclosure subjected to intermittent heating from the side. Previous studies, considering an enclosure filled with fluid or with a fluid saturated porous medium having a Prandtl number equal to seven, have demonstrated the existence of convection resonance when the heat pulsating frequency approaches the natural flow frequency of the system. The natural frequency of the flow can be well estimated using a general theory valid for fluid systems and for fully saturated porous medium systems. The results presented here test the validity of the theory for estimating the resonance frequency of systems with different Prandtl number. Numerical simulations confirm the existence of a preferred (resonance) heat pulsating frequency that compares well with the theoretical estimates. They also indicate that natural convection resonance is smoothed (damped), for the same Rayleigh number and the same Darcy number (in the case of a porous medium), when the Prandtl number increases or decreases from the value $Pr \sim 1$. Analysis of the theoretical model, in line with the numerical results, indicates that the resonance frequency of a fluid or a porous medium system varies with $Pr^{1/2}$.

BACKGROUND

A very important natural thermal process is the radiation heating and cooling of the Earth. This large scale transient process affects several transport phenomena, from atmospheric (wind) currents to convection in local fluid reservoirs (lakes). The multitude of naturally occurring time dependent (oscillatory) thermal systems should justify the recent interest in this particular area of research. Moreover, there are other thermal systems and processes of artificial (man made) character (e.g. heat storage systems, materials processing, lasers, electronics) that can benefit from this fundamental research effort.

A particular class of oscillatory thermal systems is that of fluid saturated porous enclosures (building insulation, grain storage silos, heat storage systems, etc.). Only a small number of studies published in the archival literature considered this class of systems. The studies by Caltagirone [1], Chhuon and Caltagirone [2] and Rudraiah and Malashetty [3] dealt with stability or onset of convection in a fluid saturated porous medium layer under periodic vertical temperature gradient. The corresponding supercritical (convection) regime was investigated by Kazmierczak and Muley [4]. Nield [5] investigated the onset of convection in a fluid saturated porous medium under time-periodic volumetric heating.

The case of periodic horizontal heating was studied by Antohe and Lage [6] focusing on the natural convection resonance within a porous enclosure under a fixed amplitude heating. Their numerical simulations, for Pr equal to seven, covered a wide range of input heat frequencies with the Darcy number varying from 10^{-2} to 10^{-6} and the Rayleigh number varying from 10^6 to 10^{12}.

The work was later extended by Antohe and Lage [7], where the heating amplitude effect on the resonance frequency was unveiled. They also presented a general theory for predicting the resonance frequency of a fluid or of a fully saturated porous medium system, based on scale analysis. The theory was demonstrated to be an efficient tool for narrowing the frequency range of interest for the numerical simulations. Their results indicated a reduced response of a porous system to oscillatory heating as the solid matrix becomes less permeable, the response being

† Author to whom correspondence should be addressed.

NOMENCLATURE

A	nondimensional heating amplitude, Fig. 1
Da	Darcy number, equation (7)
f, F	dimensional and nondimensional frequencies, $F=(2\Omega)^{-1}$
g	acceleration of gravity [m s^{-2}]
H	enclosure height [m]
i	iteration index
I	Forchheimer inertia coefficient, equation (8)
L	enclosure length [m]
J	viscosity ratio, equation (6)
k	thermal conductivity [W m^{-1} K^{-1}]
K	permeability [m^2]
Nu	mid-plane averaged Nusselt number, equation (9)
p, P	dimensional and nondimensional pressures, equation (5)
Pr	Prandtl number, equation (7)
q'', Q''	dimensional and nondimensional heat fluxes, Fig. 1 and equation (8)
Ra	Rayleigh number, equation (8)
t	time [s]
T	temperature [K]
u, v	horizontal and vertical seepage (Darcy) velocity components, Fig. 1 [m s^{-1}]
U, V	nondimensional horizontal and vertical velocity components, equations (5)
x, y	horizontal and vertical coordinates, Fig. 1 [m]
X, Y	nondimensional horizontal and vertical coordinates, equation (5).

Greek symbols

α	thermal diffusivity, equation (7) [m^2 s^{-1}]
β	isobaric coefficient of thermal compressibility [K^{-1}]
Δ	difference
ε	dummy variable, equation (15)
ϕ	porosity
λ	volumetric specific heat ratio, equation (7)
μ	dynamic viscosity [kg m^{-1} s^{-1}]
ν	kinematic viscosity [m^2 s^{-1}]
θ	nondimensional temperature, equation (6)
ρ	density [kg m^{-3}]
τ	nondimensional time, equation (6)
ξ	auxiliary function
Ω	nondimensional heating half-period
Ψ	streamfunction.

Subscripts

D	porous modified
f	fluid
h	high-heating regime
H	heated wall
ℓ	low-heating regime
m	reference value
M	mid-vertical plane
max	maximum Nu amplitude value
opt	optimum (resonance) frequency
p	solid porous matrix
s	porous medium (fluid and solid matrix)
ss	steady state
v	flow
0	initial.

Superscripts

$(\bar{\ })$	surface averaged.

undetectable when $Da \leqslant 10^{-6}$, within the Ra range investigated.

Lage and Bejan [8] discussed briefly the effect of oscillatory heating an enclosure filled with different Prandtl number fluids. We now extend the analysis to the fully saturated porous medium case with the main objective of testing the validity of the theoretical model presented by Antohe and Lage [7] for estimating the resonance frequency of systems with different Prandtl numbers.

FORMULATION

Consider an isotropic, rigid, porous medium square enclosure filled with a Newtonian fluid. The top and bottom surfaces of the enclosure are adiabatic and one wall is maintained at a constant temperature, equal to the initial temperature (T_0) of the quiescent fluid and solid matrix. A constant and uniform heat flux (q''_m) is imposed to the opposite wall. After an initial evolution of the system to a steady state, the heat flux starts to pulsate around its initial value following a square (high/low) wave of fixed amplitude (Aq''_m) and frequency $(\Delta t_h + \Delta t_\ell)^{-1}$ (Fig. 1). The evolution of the system, assuming the Oberbeck–Boussinesq approximation and local thermal equilibrium between the fluid and the solid matrix, is governed by the nondimensional, time dependent, general conservation of mass, momentum and energy equations (Antohe and Lage [7]), written in Cartesian coor-

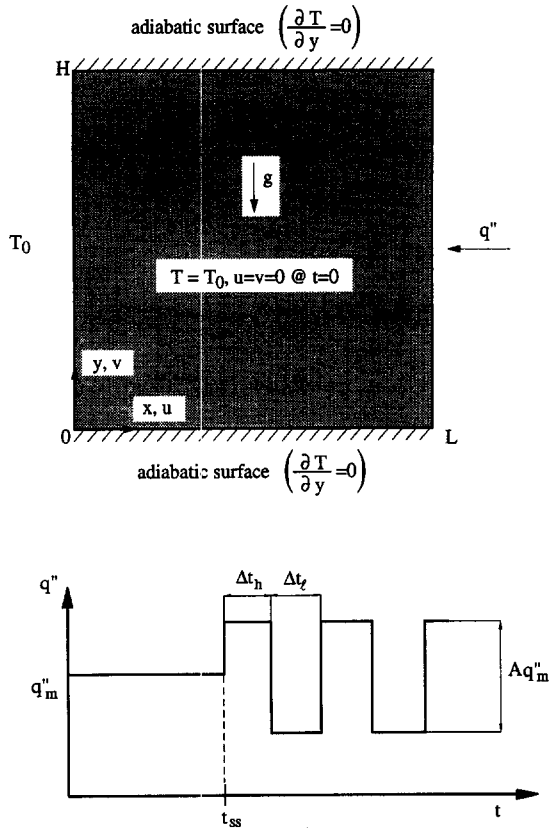

Fig. 1. Enclosure filled with fluid or with fluid saturated porous medium, boundary and initial conditions, and pulsating heat parameters.

dinates, respectively:

$$\frac{\partial U}{\partial X}+\frac{\partial V}{\partial Y}=0 \tag{1}$$

$$\frac{DU}{D\tau}=-\frac{\partial P}{\partial X}+\phi Pr J\nabla^2 U-\phi^2\frac{I}{Da}(U^2+V^2)^{1/2}U-\phi^2\frac{Pr}{Da}U \tag{2}$$

$$\frac{DV}{D\tau}=-\frac{\partial P}{\partial Y}+\phi Pr J\nabla^2 V-\phi^2\frac{I}{Da}(U^2+V^2)^{1/2}V-\phi^2\frac{Pr}{Da}V+\phi^2 Ra\,Pr\theta \tag{3}$$

$$\frac{\lambda}{\phi}\frac{\partial\theta}{\partial\tau}+U\frac{\partial\theta}{\partial X}+V\frac{\partial\theta}{\partial Y}=\nabla^2\theta, \tag{4}$$

and appropriate boundary conditions (the thermal boundary conditions and the initial conditions are shown in Fig. 1; the continuity and momentum boundary conditions are the nonslip and impermeable conditions at the solid surfaces).

Lage [9] showed that the transient decay time of the convective momentum transport in porous media is proportional to $Da/(\phi^2 Pr)$ for Darcy flow, and to $Da^{3/4}/(\phi^{3/2}Ra_D Pr)^{1/2}$ for Forchheimer flow. Then, when considering systems with high Darcy number values, the transient flow inertia term should not be neglected *a priori*. The nondimensional variables, with corresponding dimensional quantities listed in the nomenclature, are:

$$(X, Y)=\frac{(x, y)}{H}\quad (U, V)=\frac{(u, v)}{\alpha_s/H}$$

$$P=(p+\rho_f g y)\frac{\phi^2 H^2}{\rho_f\alpha_s^2} \tag{5}$$

$$\theta=\frac{T-T_0}{q''_m H/k_s}\quad \tau=\frac{t-t_{ss}}{\phi H^2/\alpha_s}\quad J=\frac{\mu_s}{\mu} \tag{6}$$

$$\lambda=\frac{(\rho c)_s}{(\rho c)_f}\quad Pr=\frac{\nu}{\alpha_s}\quad \alpha_s=\frac{k_s}{(\rho c)_f}\quad Da=\frac{K}{H^2} \tag{7}$$

$$Ra=\frac{g\beta q''_m H^4}{\nu\alpha_s k_s}\quad I=1.75\left(\frac{Da}{150\phi^3}\right)^{1/2}\quad Q''=\frac{q''}{q''_m}. \tag{8}$$

Our interest is restricted to the oscillating heating process so the dimensionless time is shifted to zero when the pulsating regime starts (t_{ss} is the warm-up time of the system to reach steady state at the end of the initial regime, Fig. 1). Parameter J, equation (6), accounts for the effective viscosity of the fluid saturated porous medium, Cheng [10]. The expression for the inertia parameter, I, shown in equation (8), follows the Ergun [11] model. Observe that the Navier-Stokes equations and the energy fluid equation are recovered from equations (2)–(4) by simply setting $Da\to\infty$, $\phi=\lambda=J=1$, and substituting all the porous medium properties $()_s$ by the corresponding fluid properties $()_f$.

Notice that the Rayleigh number defined in equation (8) is based on a reference value of the pulsating heat flux, q''_m. The instantaneous time dependent Rayleigh number is then equal to $Ra\,Q''$. A porous modified heat flux based Rayleigh number, Ra_D, is defined as equal to $Ra\,Da$.

Here, the nondimensional heat pulsation amplitude A is kept at 40% of the reference value. Therefore the system is always being heated at the heating wall, but with time-varying heating intensity. We set equal high-heating and low-heating time intervals, $\Omega_h=\Omega_\ell=\Omega$, so the nondimensional heat pulsating frequency is: $F=1/(2\Omega)$. We note in passing that the simplified (boundary layer) analysis presented by Vargas and Bejan [12] indicated that equal high heating and low heating periods optimize the heat transfer process of pulsating heat along a vertical surface. According to the definition of dimensionless time, equation (6), and Fig. 1, the dimensional high-heating and low-heating time intervals are, respectively: $(\Delta t_h, \Delta t_\ell)=(\Omega_h, \Omega_\ell)\,\phi H^2/\alpha_s$, for the porous medium case, and $(\Delta t_h, \Delta t_\ell)=(\Omega_h, \Omega_\ell)H^2/\alpha_f$, for the fluid case.

The representative parameter for monitoring the convection strength inside the enclosure is the instan-

taneous surface-averaged heat transfer rate across an imaginary vertical plane positioned at the mid-distance from the vertical surfaces of the enclosure, q''_M. The corresponding nondimensional quantity is

$$Nu = \frac{\bar{q}''_M}{q''_m} = \int_0^1 \left(U\theta - \frac{\partial \theta}{\partial X} \right)_{X=L/(2H)} \mathrm{d}Y. \quad (9)$$

THEORETICAL ANALYSIS

The parameter space of the present problem is large. Even considering a specific case, fixing all parameters but the heat pulsating frequency, the probability of choosing an input heat frequency near the resonance frequency is very small. It is obvious that any analysis leading to a reasonable estimate of the resonance frequency is welcome. A theoretical representation of the flow wheel frequency, f_v, was introduced by Antohe and Lage [6] for clear fluid and porous medium configurations, assuming a single fluid circulating speed (valid during a complete heating cycle) based on the cycle-averaged Rayleigh number. Their approach led to a simple closed-form estimate of the resonance frequency.

A more consistent and general theory was developed by Antohe and Lage [7] recognizing that different fluid circulating speeds are induced during each heating interval. The corresponding cycle-averaged velocity is different than the velocity induced by the cycle-averaged Rayleigh number (the velocity scale is a nonlinear function of the Rayleigh number). Although more laborious, this approach was shown to yield more accurate estimates of the resonance frequency by including the heating amplitude effect (the result presented by Antohe and Lage [6] is independent of the heating amplitude). The extra effort is translated, eventually, into fewer numerical simulations for establishing the precise resonance frequency of the system.

Their theory is fundamental because it provides some guidance to the task of pinpointing the resonance heating frequency f_{opt}. Only the results of their derivation are presented here, the details can be found in Antohe and Lage [7]. The basis of their analysis is the physical principle that resonance can be induced in vibrating systems when the forcing (heating) frequency, f, coincides with the natural frequency of the system, f_v. The natural frequency of our present system, in nondimensional form, is the flow wheel frequency related to the fluid velocity scale during each heating interval as:

$$F_v = \frac{1}{(\Omega_h + \Omega_\ell)} \sim \frac{V_h + V_\ell}{4\left(1 + \dfrac{L}{H}\right)}. \quad (10)$$

Each velocity can be obtained from the momentum equation in scale form, for a fluid saturated porous medium system:

$$V_{h,\ell}^2 \left[1 + \phi J\, Pr \xi(Pr) + \frac{0.143\phi^{1/2}}{Da^{1/2}} \right] + V_{h,\ell} \left[\frac{1}{\Omega_{h,\ell}} + \frac{\lambda}{\Omega_{h,\ell}} J\, Pr \xi(Pr) + \frac{\phi^2 Pr}{Da} \right] - \phi^2 Ra\, Pr \xi(Pr)^{-1/2} \bar{\theta}_{H_{h,\ell}} \sim 0 \quad (11)$$

and for a clear fluid system

$$V_{h,\ell}^2 [1 + Pr\xi(Pr)] + V_{h,\ell} \left[\frac{1}{\Omega_{h,\ell}} + \frac{1}{\Omega_{h,\ell}} Pr\xi(Pr) \right] - Ra\, Pr \xi(Pr)^{-1/2} \bar{\theta}_{H_{h,\ell}} \sim 0 \quad (12)$$

with $\xi(Pr)$ equal to 1 for $Pr \geqslant 1$, or to Pr^{-1} for $Pr \leqslant 1$. When combined with the heating wall temperature scale (Antohe and Lage [7]), for a porous medium:

$$\bar{\theta}_{H_{h,\ell}} \sim 2.34\phi^{0.3} \frac{L}{H} (Ra_{h,\ell} Pr)^{-1/5} Da^{-1/10} \quad (13)$$

and for a clear fluid medium

$$\bar{\theta}_{H_{h,\ell}} \sim \frac{L}{H} Ra_{h,\ell}^{-1/5}\, \xi(Pr)^{1/5} \quad (14)$$

where here the high-heating and low-heating instantaneous Rayleigh numbers, Ra_h and Ra_ℓ, are equal to $(1 + A/2)Ra$ and $(1 - A/2)Ra$, respectively (note: $Ra_{h,\ell} = RaQ''_{h,\ell}$).

Equation (10) and equations (11) and (13) for a porous medium, or equations (12) and (14) in the case of a clear fluid system, form a system of algebraic and coupled nonlinear equations in the unknowns $F_v = 1/(2\Omega)$, V_h and V_ℓ. The system of equations is solved numerically for each particular set of parameters. Within the parametric range considered here, the numerical solution of the system of equations leads to four real solutions. Two of them are negative and are immediately discarded. The correct answer, the resonance frequency F_{opt}, is selected among the remaining two by enforcing the positive velocity scale requirement (the scale analysis is done along the heating wall where the fluid vertical velocity scale is positive). Only one of the two remaining solutions satisfies this requirement.

NUMERICAL METHOD AND RESULTS

Numerical results are obtained by solving the system of time dependent differential equations (1)–(4), with appropriate boundary and initial conditions, using the finite volume method, Patankar [13]. The discretized equations are solved using the SIMPLE algorithm with a fully implicit alternating-direction Gauss–Seidel method, and the efficient tri-diagonal-matrix Thomas algorithm. The present code was validated by comparing the results against the results reported by Armfield and Patterson [14].

Nonuniform grid accuracy tests are performed attending for the basic concepts presented in detail by

Manole and Lage [15]. Several different grid distributions are implemented, depending on the parametric configuration, using never less than 60 grid lines in each direction. Numerical results reported here are at least 5% accurate based on a 50% increase in the total number of grid lines. The quantitative results of grid accuracy tests are too comprehensive to be presented here because they involve varying two variables (total number of grid points and grid base size, Manole and Lage [15]) for each physical configuration characterized by Pr, Ra, Da, and F. Moreover, a comprehensive study on this subject is in preparation by the authors and it will be submitted for publication in the future.

Convergence of the numerical iterations is achieved when the local criterion

$$\mathrm{MAX}\left|\frac{\varepsilon^{i+1}-\varepsilon^{i}}{\varepsilon^{i}}\right| < 10^{-3} \tag{15}$$

is satisfied. In equation (15) ε represents all three main variables, U, V and θ, at every location of the discretized domain. The indexes i and $i+1$ are any two consecutive iterations at the same time τ. To obtain results that are insensitive to the time step selected (time discretization error much smaller than convergence criterion) a minimum of 400 time iterations are performed during each heating cycle.

The parameter λ/ϕ of equation (4) is set equal to one ($\phi = 0.4$, $\lambda = 0.4$), a reasonable approximation for values obtained in practical systems, e.g. glass–water 1.33, soil–water 1.24. From $(\rho c)_s = \phi(\rho c)_f + (1-\phi)(\rho c)_p$, one can show that $\lambda = \phi$ is the limiting case of an adiabatic solid matrix. Therefore, the results presented here are valid also for concentration driven convection, if one replaces temperature with concentration and all the thermal parameters with the corresponding solutal parameters.

We note in passing that for values of λ/ϕ larger than one the thermal inertia of the system increases, that is, the system responds slower in time to temperature variations. We do not believe that using the λ/ϕ values listed in the previous paragraph would significantly alter our present results because the Prandtl number values we consider are relatively low. In this case, the energy balance is mainly between convection and diffusion. However, for very high-Pr systems the thermal inertia term might predominate, and consequently, variations in the λ/ϕ value can become important.

Figure 2 presents a sample of the numerical results for three distinct heating frequencies with $Da = 10^{-4}$, $Ra = 10^{12}$ and $Pr = 0.02$. The convection process inside the enclosure develops to a periodic regime after a certain number of heating cycles (the exact number of cycles depends upon the parametric configuration). Only two consecutive cycles of the developed periodic regime are displayed in Fig. 2. In all cases $L/H = 1$, $A = 0.4$, and $J = 1$. Observe the series of ripples in the Nu curve developed during each heating interval

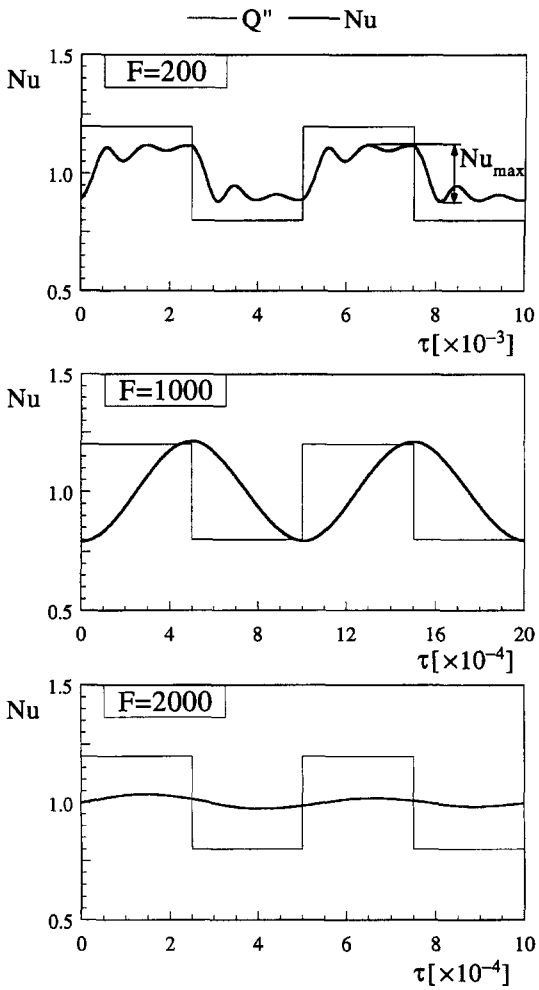

Fig. 2. Time evolution of mid-plane Nusselt number for $Da = 10^{-2}$, $Ra = 10^{12}$, $Pr = 0.02$.

of the low frequency case $F = 200$ (top graph). The intensity of the system response to the periodic heating Q'' is indicated by the maximum Nusselt number amplitude, Nu_{max}, measured as indicated in the top graph. As the heating frequency increases to 1000 (middle graph) the ripples disappear and the Nusselt amplitude increases slightly beyond the heating amplitude. A further increase in the heating frequency, bottom graph for $F = 2000$, yields a drastic drop in the Nusselt amplitude.

In Fig. 3 we show results also for $Da = 10^{-4}$ and $Ra = 10^{12}$, but with $Pr = 0.7$. Again in this case, ripples are present in the Nu curve of the low heating frequency F = 1250 (top) graph. The ripples disappear when the frequency is increased to $F = 4166$ (middle graph) and the Nusselt amplitude increases well beyond the heating amplitude and the Nu amplitude of $Pr = 0.02$ case shown in Fig. 2 (top). The bottom graph of Fig. 3, for $F = 5000$, presents a reduction in the Nusselt amplitude and no ripples.

The graphs in Figs. 2 and 3 indicate that the concept of resonance frequency introduced by Lage and Bejan

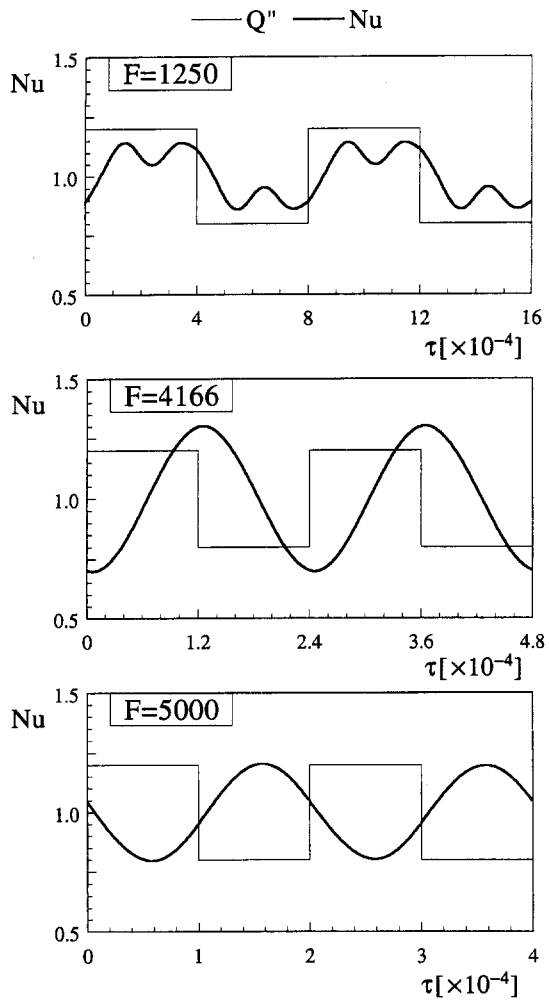

Fig. 3. Time evolution of mid-plane Nusselt number for $Da = 10^{-2}$, $Ra = 10^{12}$, $Pr = 0.7$.

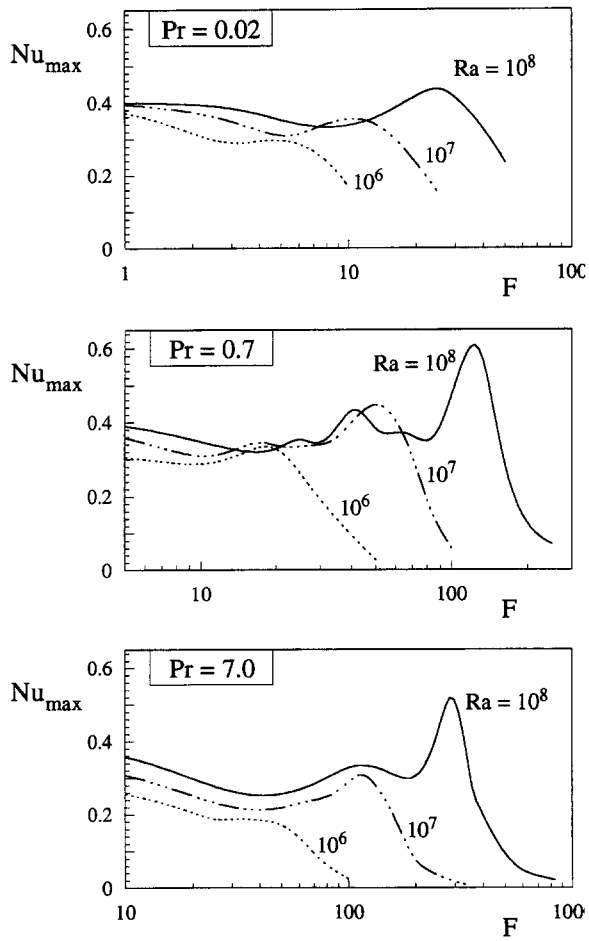

Fig. 4. Prandtl number effect on thermal response of porous medium enclosure with $Da = 10^{-2}$.

(1993) for a $Pr = 7$ medium can be extended to porous systems with different Pr. The graphs also show a distinct dependency of the convective response (Nu) to the heating frequency (F) for systems with different Prandtl number.

Figures 4 and 5 show how the maximum value of the mid-plane averaged Nusselt number amplitude varies with the heating frequency F, for $Da = 10^{-2}$ (Fig. 4) and for $Da = 10^{-4}$ (Fig. 5). The Rayleigh number range is 10^6–10^8 for Darcy number 10^{-2}, and 10^{10} to 10^{12} for Darcy number 10^{-4}. Notice that the corresponding porous-modified Rayleigh number (Ra_D) range is 10^4–10^6 for Darcy number 10^{-2}, and 10^6 to 10^8 for Darcy number 10^{-4}. The Prandtl number of the porous system varies, being equal to 0.02 (top graph), 0.7 (middle graph) and 7 (bottom graph). No evidence of resonance was detected for low permeability media ($Da \leqslant 10^{-6}$), with Rayleigh numbers as high as 10^{14} ($Ra_D = 10^8$).

From top to bottom, the graphs of Figs. 4 and 5 indicate the effect of increasing the Prandtl number. Notice in Fig. 4 that lowering Prandtl number has the effect of 'diffusing' the response of the system to periodic heating. That is, the Nusselt number amplitude variation with heating frequency becomes smoother as Pr decreases from 7 to 0.7, and further on to 0.02.

A common feature of both figures is the variation on the number of 'peaks' of each Ra curve. For instance, in Fig. 4 for $Ra = 10^8$, there is only one peak when $Pr = 0.02$, then four peaks are apparent when $Pr = 0.7$, and only two when $Pr = 7$. In Fig. 5, for $Ra = 10^{12}$, the number of peaks is 2, 4 and 2 for Prandtl number 0.02, 0.7, and 7, respectively. This indicates that the system becomes 'stiffer' to pulsating heat excitation by either increasing or decreasing Pr from 0.7.

Another common feature is the location of the resonance frequency, that is the frequency leading to the maximum average Nusselt number amplitude. For each Ra value the location of the resonance frequency moves to the right (increased frequency) as Pr increases from 0.02 to 0.7, and from 0.7 to 7.

Several resonance frequency results are presented in Table 1. Some numerical results (indicated with an asterisk) of an enclosure filled with fluid only (no

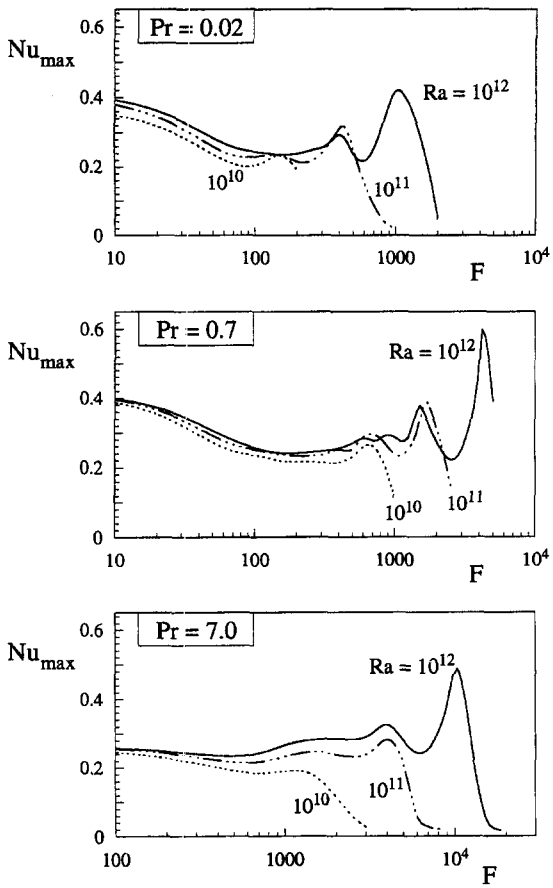

Fig. 5. Prandtl number effect on thermal response of porous medium enclosure with $Da = 10^{-4}$.

porous medium) obtained by Lage and Bejan [8] are included for completeness. Notice that all theoretical estimates are obtained with the general model reviewed in the previous section.

The theoretical estimates are within a factor of order one from the numerical results, being consistently smaller. The deviation seems to increase slightly as the Prandtl number and/or the Darcy number decrease. These results are remarkable considering the general mathematical simplicity of the theoretical approach (scale analysis) and that the flow inside the enclosure is very complex and the phenomenon highly nonlinear.

Notice in Table 1 how the resonance frequency is reduced as the Prandtl number decreases. This does not indicate that the thermo-hydraulic response of the system to pulsating heating is slowed down. If one compares, for the same configuration (ν, H, ϕ), the physical (dimensional) heating period ratio for systems with different Prandtl numbers, say Pr_1 and Pr_2, the result is

$$\frac{\Delta t_{Pr_1}}{\Delta t_{Pr_2}} = \frac{F_{Pr_2}}{F_{Pr_1}} \frac{Pr_1}{Pr_2}. \tag{16}$$

From Table 1 one can observe that the equivalent dimensional resonance heating period decreases as the Prandtl number of the system decreases. From $Pr_1 = 7$ to $Pr_2 = 0.7$, for instance with $Da = 10^{-4}$ and $Ra = 10^{12}$, the porous system resonance frequency drops approximately 2.5 times, that is $F_{Pr_1} = 2.5\, F_{Pr_2}$. The optimum dimensional heating period of $Pr_2 = 0.7$, from equation (16), is about five times smaller than the optimum heating period of $Pr_1 = 7$. Similar calculations indicate that the optimum heating period becomes approximately eight times smaller if the Prandtl number goes from $Pr = 0.7$ to $Pr = 0.02$. The corresponding changes in the clear fluid system are less dramatic, being approximately one and a half times smaller for $Pr = 0.7$ than for $Pr = 7$, and about six times smaller from $Pr = 0.7$ to $Pr = 0.01$. It is true then that the system responds faster to the pulsating heating when Pr is reduced.

To look closer into the Prandtl number effect on the

Table 1. Comparison between numerical and theoretical resonance (optimum) frequencies ($H/L = 1, \phi = 0.4, \lambda = 0.4, J = 1$)

	Clear fluid				$Da = 10^{-2}$			$Da = 10^{-4}$	
$Pr = 7$									
Ra	10^7	10^8	10^9	10^6	10^7	10^8	10^{10}	10^{11}	10^{12}
Numerical	250	588	1666	33	114	294	1219	4000	10000
Theoretical	120.7	303.3	761.9	18.7	48.0	120.8	562.6	1484.5	3799.2
Numerical/theoretical	2.07	1.94	2.19	1.76	2.38	2.43	2.17	2.69	2.63
$Pr = 0.7$									
Ra	10^6	10^7	10^8	10^6	10^7	10^8	10^{10}	10^{11}	10^{12}
Numerical	41.8*	105.8*	209.2*	18	50	125	625	1613	4166
Theoretical	28.8	72.4	181.8	10.6	26.3	65.1	247.3	628.9	1584.3
Numerical/theoretical	1.45	1.46	1.15	1.70	1.90	1.92	2.53	2.56	2.63
	$Pr = 0.01$				$Pr = 0.02$			$Pr = 0.02$	
Ra	10^6	10^7	—	10^6	10^7	10^8	10^{10}	10^{11}	10^{12}
Numerical	8*	14.9*	—	5	10	25	152	417	1000
Theoretical	1.8	4.6	—	1.2	2.8	6.7	25.7	63.9	159.3
Numerical/theoretical	4.44	3.24	—	4.17	3.57	3.73	5.91	6.53	6.28

* From Lage and Bejan ref [8]. Note that the results from ref. [8] need to be transformed using $F = F_{L\&B}\,(Ra\,Pr)^{1/2}$ due to the different time scale used by the authors.

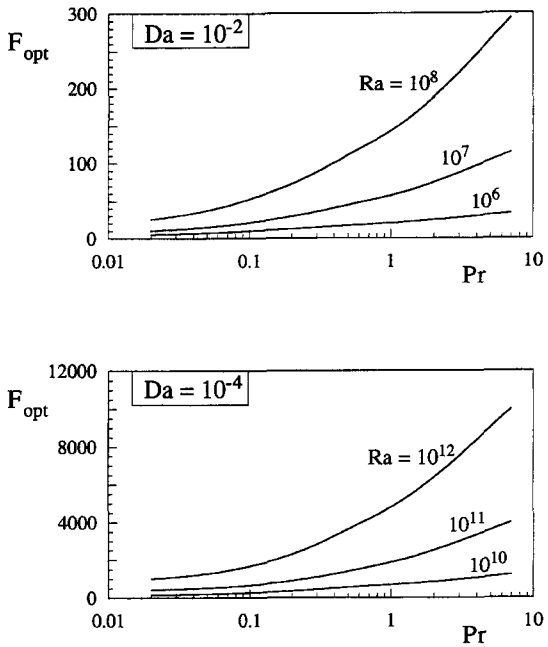

Fig. 6. Optimum (resonance) frequency vs Prandtl number.

resonance frequency we present in Fig. 6 the optimum (resonance) frequency F_{opt} of each porous system ($Da = 10^{-2}$ top, and $Da = 10^{-4}$ bottom) vs the Prandtl number. We noticed the similar shape of the curves in each graph, and this prompted us to go back to the theoretical analysis and investigate the functional dependency of F_v and Pr. Unfortunately, the scheme proposed by Antohe and Lage [7] requires the numerical solution of a system of equations to find F_v. However, the simpler analysis presented by Antohe and Lage [6] leads to a close form solution for F_v. Neglecting the Brinkman effect (correct on a scale sense) and assuming that the Darcy effect is negligible (notice we are dealing here with reasonably high Darcy number values) the expression for F_v from Antohe and Lage [6] is simplified to:

$$F_v \sim \frac{\phi}{8}\frac{\left[4\phi^2 Ra^{4/5} Da^{-1/10} Pr\left(1+\dfrac{0.143\phi^{1/2}}{Da^{1/2}}\right)\right]^{1/2}}{\left(1+\dfrac{0.143\phi^{1/2}}{Da^{1/2}}\right)}. \tag{17}$$

The two terms within parentheses refer to the convective inertia and to the Forchheimer effects, respectively. The next step is to assume either case separately, that is, consider a predominating convective inertia effect and obtain

$$F_v \sim \phi^2 Pr^{1/2} Ra_D^{2/5} Da^{-9/20}. \tag{18}$$

Next, consider the Forchheimer effect predominating over the inertia effect and find

$$F_v \sim \left[\frac{\phi^{9/4}}{4(0.143)^{1/2}}\right] Pr^{1/2} Ra_D^{2/5} Da^{-4/20}. \tag{19}$$

The group $(Pr^{1/2} Ra_D^{2/5})$ appears in both cases, indicating that the resonance frequency varies with the square root of the Prandtl number. The main difference between these two extreme cases resides in the Darcy exponent, equal to -0.45 $(-9/20)$ for predominating convective inertia and to -0.20 $(-4/20)$ if Forchheimer predominates. We compare both options with the numerical results and obtain the best agreement when the exponent is equal to -0.35 $(-7/20)$, that is close to the average value of the other two. We demonstrate the accuracy of this result in Fig. 7, where $F_{opt}/(Da^{-7/20} Ra_D^{2/5})$ is plotted (using the numerical values of F_{opt} from Table 1) against $Pr^{1/2}$ for several configurations. The straight line indicates how well the predicted Pr dependency correlates the numerical results. It also provides the correct constant for the final equation

$$F_{opt} = 0.09 Da^{-7/20} Ra_D^{2/5} Pr^{1/2}. \tag{20}$$

The deviation of cases $Da = 10^{-2}$ and $Ra = 10^6$, and $Da = 10^{-4}$ and $Ra = 10^{10}$, at $Pr = 7$ (shown next to the brace), might result from the uncertainties associated with determining precisely the resonance values for these cases by numerical simulations. Revisiting Figs. 4 and 5 one notices that the Nu vs F curves for these cases are relatively flat which makes the precise determination of the resonance frequency value very demanding. The deviation is not very important because the resonance is very weak for these two cases anyhow.

It is worth comparing equation (20) with the results obtained by Lage and Bejan [8] for a fluid enclosure. Using the present nomenclature, their results are $F_{opt} \sim Ra^{2/5}$ if $Pr > 1$, and $F_{opt} \sim Ra^{2/5} Pr^{2/5}$ if $Pr \leqslant 1$. Notice that the Ra effect is basically the same. The dual Pr effect is a consequence of the momentum diffusion term that can not be neglected when dealing with a fluid system.

Figures 8 and 9 present the evolution of the streamlines and isotherms, respectively, during one heating cycle at resonance heating frequency for $Da = 10^{-2}$ and $Ra = 10^8$. The cases of $Pr = 0.02$, 0.7 and 7 are seen side by side for comparison. The streamlines and isotherms are equally spaced in all cases. The frames of each figure form a time sequence proportional to the half-heating period Ω (or to the heating frequency, $F = 1/2\Omega$) of each configuration as indicated to the left of the frames. The sequence starts at the beginning of the high heating cycle. These figures help understand why the thermal response of the system (resonance intensity) decreases either by increasing or decreasing Pr from 0.7.

We initially notice that the Prandtl number value of 0.7 is the closest to an equilibrium between viscous and thermal diffusivities (ideally, $Pr = 1$). As the Pr value deviates from this equilibrium value the system's

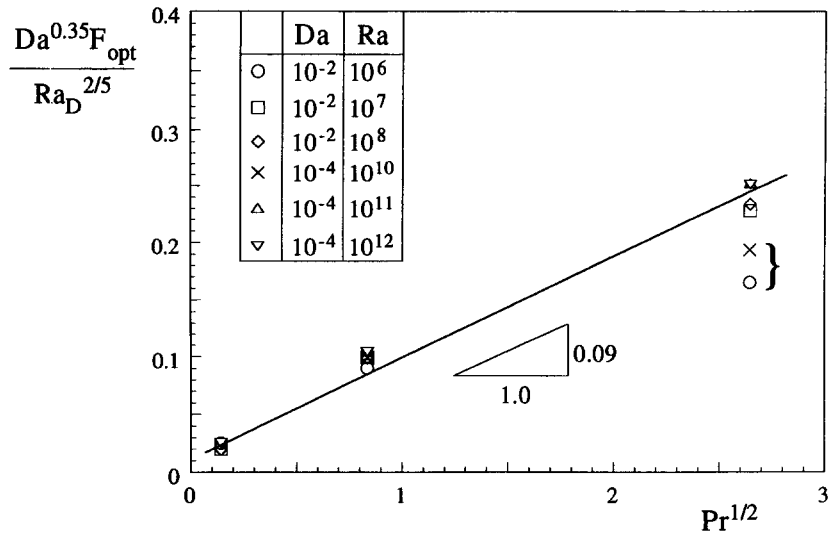

Fig. 7. Verification of functional dependence of resonance frequency, Darcy number, Darcy-modified Rayleigh number, and Prandtl number.

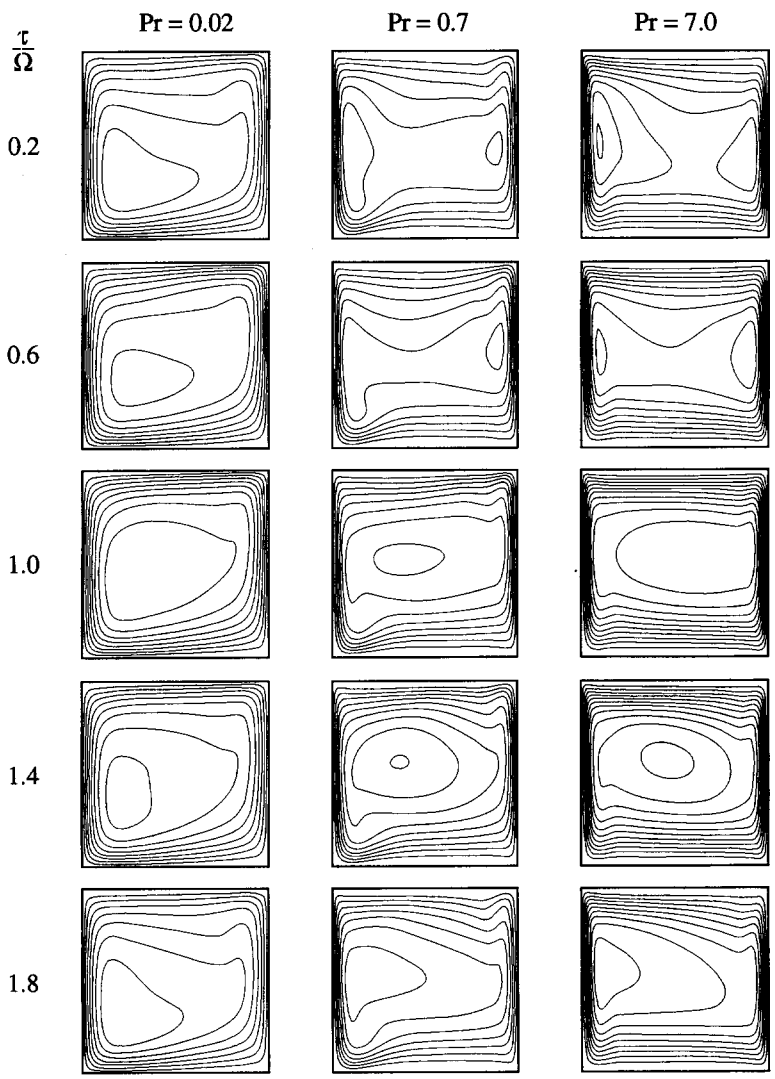

Fig. 8. Streamlines from numerical simulations for $Da = 10^{-2}$, $Ra = 10^{8}$. The corresponding heating frequency of each Pr case is found in Table 1.

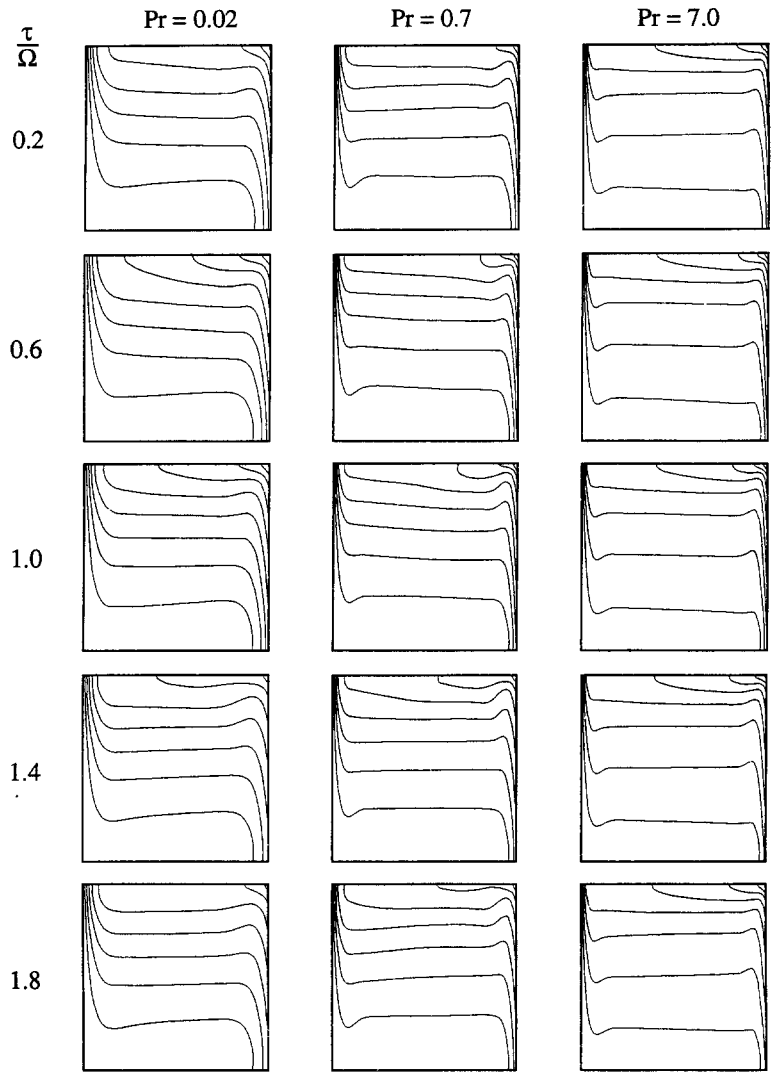

Fig. 9. Isotherms from numerical simulations for $Da = 10^{-2}$, $Ra = 10^{8}$. The corresponding heating frequency of each Pr case is found in Table 1.

response is hindered. We hypothesize that the system response is related to a dual and equivalent effect of viscous and thermal diffusivities.

Consider for instance the case $Pr < 1$, where thermal diffusivity prevails. In this case, with high heat diffusion, the heat transferred to the enclosure (same for all cases of Figs. 8 and 9 because the Rayleigh number value is the same in all cases) can be transported with smaller temperature gradients than for $Pr \geqslant 1$ (see how the isotherms of $Pr = 0.02$, Fig. 9, are smoother and more distant from the walls than those of Pr 0.7 and 7). But smaller temperature gradients reduce buoyancy which reduces the natural convection strength within the enclosure. Observe that only one distinct flow cell is visible during the heating cycle of $Pr = 0.02$, while two flow cells are present for $Pr = 0.7$ and $Pr = 7$. We can then expect the $Pr < 1$ system to be less responsive to periodic heating.

A system with $Pr > 1$ entails a strong viscous diffusion mechanism, that is, a large portion of fluid moves with smaller speed for the same inertia (thicker momentum boundary layers). The viscous drag effect of the porous medium is also increased. In this case the natural convection strength is expected to be reduced as well because the buoyancy-induced inertia is diffused through a larger fluid region and more effectively dissipated (notice how the bouncing-like effect of the upward flow jet in the top right region of the frames in Fig. 8, for $Pr = 0.7$, is minimized when $Pr = 7$). Therefore, the system convective response is also reduced when $Pr > 1$.

In conclusion, systems with $Pr \sim 1$ provide a better balance between thermal and viscous diffusion when it comes to convective strength under time periodic heating.

CONCLUSIONS

The Prandtl number effect on the natural convection response of enclosures filled with a fluid satu-

rated porous medium, and under pulsating heating from one side, is investigated and compared with the Prandtl number effect on the response of fluid filled enclosures. The convection activity is monitored with the surface averaged heat transfer crossing the midplane of the enclosure. As the frequency of heat pulsation increases the heat transfer amplitude presents several local maxima. The heating frequency of maximum response (highest heat flux amplitude) is referred to as the resonance heating frequency of the system.

The resonance frequency value of porous systems varies with $Pr^{1/2}$, as predicted theoretically and confirmed numerically. Moreover, the convection activity inside the enclosure decreases when Pr is increased or decreased from a value of order one. This phenomenon is explained physically by considering the hindering effect of a more viscous system (high Pr) on the convection inside the enclosure, and the damping effect of a higher thermal diffusivity system (low Pr) via smoothed temperature gradients and reduced buoyancy (convection). Evidence supporting these hypotheses is presented by the time evolution of streamlines and isotherms during one heating cycle, for systems having a Prandtl number equal to 0.02, 0.7 and 7.

Acknowledgements—Financial support provided by NSF through grant no. CTS-9504968 is greatly appreciated. Dr Antohe expresses his gratitude for the Ph.D. scholarship provided by the Mechanical Engineering Department of Southern Methodist University. Professor Lage is grateful also for the support provided by the J. L. Embrey Professorship in Mechanical Engineering.

REFERENCES

1. Caltagirone, J. P., Stabilité d'une couche poreuse horizontale soumise a des conditions aux limites périodiques. *International Journal of Heat and Mass Transfer*, 1976, **19,** 815–820.
2. Chhuon, B. and Caltagirone, J. P., Stability of a horizontal porous layer with timewise periodic boundary conditions. *Journal of Heat Transfer*, 1976, **98,** 49–54.
3. Rudraiah, N. and Malashetty, M. S., Effect of modulation on the onset of convection in sparsely packed porous layer. *Journal of Heat Transfer*, 1990, **112,** 685–689.
4. Kazmierczak, M. and Muley, A., Steady and transient natural convection experiments in a horizontal fluid layer: the effects of a thin top fluid layer and oscillating bottom wall temperature. *International Journal of Heat & Fluid Flow*, 1994, **15,** 30–41.
5. Nield, D. A., Onset of convection in a porous medium with nonuniform time-dependent volumetric radiation. *International Journal of Heat & Fluid Flow*, 1995, **16,** 217–222.
6. Antohe, B. V. and Lage, J. L., A dynamic thermal insulator: inducing resonance within a fluid saturated porous medium enclosure heated periodically from the side. *International Journal of Heat and Mass Transfer*, 1994, **37,** 751–782.
7. Antohe, B. V. and Lage, J. L., Amplitude effect on convection induced by time-periodic horizontal heating. *International Journal of Heat and Mass Transfer*, 1996, **39,** 1121–1133.
8. Lage, J. L. and Bejan, A., The resonance of natural convection in an enclosure heated periodically from the side. *International Journal of Heat and Mass Transfer*, 1993, **36,** 2027–2038.
9. Lage, J. L., On the theoretical prediction of transient heat transfer within a rectangular fluid-saturated porous medium enclosure. *Journal of Heat Transfer*, 1993, **115,** 1069–1071.
10. Cheng, P., Heat transfer in geothermal systems. *Advances in Heat Transfer*, 1978, **14,** 1–105.
11. Ergun, S., Fluid flow through packed columns. *Chemical Engineering Progress*, 1952, **48,** 89–94.
12. Vargas, J. V. C. and Bejan, A., Optimization Principle for Natural Convection Pulsating Heating. *Journal of Heat Transfer*, 1995, **117,** 942–947.
13. Patankar, S. V., *Numerical Heat Transfer and Fluid Flow*. Hemisphere, Washington, 1980.
14. Armfield, S. W. and Patterson, J. C., Direct simulation of wave interactions in unsteady natural convection in a cavity. *International Journal of Heat and Mass Transfer*, 1991, **34,** 929–940.
15. Manole D. M. and Lage, J. L., Nonuniform grid accuracy test applied to the natural convection flow within a porous medium cavity. *Numerical Heat Transfer—B*, 1993, **23,** 351–368.